ACS OMEGA

http://pubs.acs.org/journal/acsodf

Article

Flexible Zinc Oxide Nanowire Array/Graphene Nanohybrid for High-Sensitivity Strain Detection

Mohan Panth,* Brent Cook, Mohammed Alamri, Dan Ewing, Amy Wilson, and Judy Z. Wu*

Cite This: *ACS Omega* 2020, 5, 27359−27367

Read Online

ACCESS | Metrics & More | Article Recommendations

ABSTRACT: A fully flexible strain sensor consisting of vertically aligned ZnO nanowires on graphene transferred on polyethylene terephthalate with prefabricated Au/Ti electrodes (ZnO-VANWs/Gr)/PET) has been obtained. The ZnO-VANWs were grown in solution using a seedless hydrothermal process and are single-crystalline of (0001) orientation that provides optimal piezoelectric gating on graphene when deformed mechanically. The change of the graphene channel conductance under such a piezoelectric gating through transduction of the mechanical deformation on the ZnO-VANWs/Gr was used to detect the strain induced by the deformation. Under applied normal forces of 0.30, 0.50, and 0.70 N in a dynamic manner, the ZnO-VANWs/Gr/PET strain sensors exhibited a high response and response times of ∼0.20 s to both force on and off were achieved. Under mechanical bending curvatures of 0.18, 0.23, 0.37, and 0.45 cm^{-1}, high sensitivity of the gauge factors up to ∼248 and response times of 0.20 s/0.20 s (rise/fall) were achieved on the ZnO-VANWs/Gr/PET strain sensors. Moreover, the response changes polarity when the directions of bending alters between up and down, corresponding to the polarity change of the space charge on the ZnO-VANWs/Gr interface as a consequence of the compressive and tensile strains along the ZnO-VANWs. This result shows that the low-cost and scalable ZnO-VANWs/Gr/PET strain sensors are promising for applications in stress/strain monitoring, wearable electronics, and touch screens.

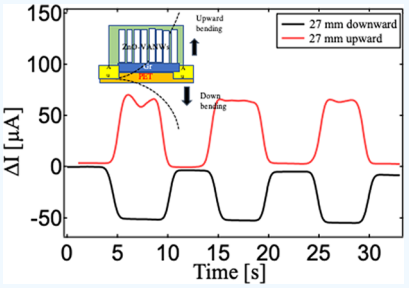

INTRODUCTION

The immense development in flexible, wearable, and self-powered electronic devices has recently emerged as the main focus of research for a large variety of applications.[1,2] Flexible/stretchable strain sensors are an excellent example and are in demanded for wearable electronics,[3] health care,[4] infrastructure monitoring,[5] robotics,[6] and so forth. Taking advantage of various functional nanomaterials, exciting progress has been made in strain sensors based on nanocomposites in the last decade or so.[7,8] Compared to traditional rigid metallic strain gauges, flexible nanocomposite strain sensors exhibit high strain tolerance, fast response, high sensitivity, low power consumption, and high sensitivity to conformal geometric changes.[8−10]

Most flexible/stretchable strain sensors rely on the piezoresistive effect, and strain sensitivity, the so-called gauge factor (G.F.), is defined by the specific conductivity change per unit strain ϵ (G.F = $(\Delta\sigma/\sigma_0)/\epsilon$).[7,11] In the case of nanocomposites, which consist of piezoelectric nanostructures,[9] such as nanoparticles (NP), nanowires (NWs), and nanotubes,[10] and so forth, mixed with polymers,[12] including polyvinylidene fluoride (PVDF), polydimethylsiloxane (PDMS), and polymethyl methacrylate (PMMA),[13−16] the sensor conductivity is measured over the entire nanocomposite sample. Various piezoelectric materials studied for strain sensors include zinc oxide (ZnO), lead zirconate titanate, and lead titanate.[17−19] In addition, filler materials, such as carbon nanotubes (CNT), carbon fibers, carbon black particles, reduced graphene oxides (rGO), and graphene (Gr),[20] have been adopted into the nanocomposites because of the high carrier mobility, flexibility, and robustness for improved conductivity and thereby sensitivity and flexibility/stretch-ability of the nanocomposite strain sensors.[8,16,21−24] Among other piezoelectric nanostructures, ZnO NWs are particularly interesting due to the high piezoelectric effect especially along the (0001)-orientation, large material abundance, non-toxic and hence environmental friendly nature, and ease in fabrication plus low fabrication cost.[25−28] Nanocomposite strain sensors based on ZnO nanostructures have been extensively studied after the pioneering work by Zhang *et al.* on converting nanoscale mechanical energy into electrical energy achieved through ZnO NWs.[29] It should be mentioned that exciting progress has been made in utilizing piezoelectric potential effectively coupled to the graphene channel for various applications such as nonvolatile memory and artificial sensory synapse.[30−33] Strain sensor of a gauge

Received: July 31, 2020
Accepted: September 28, 2020
Published: October 15, 2020

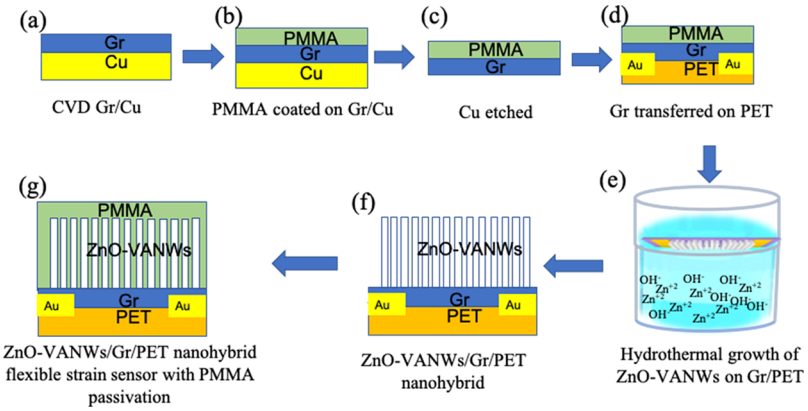

Figure 1. Schematic description of the ZnO-VANWs/Gr/PET flexible strain sensors fabrication: (a) CVD Gr grown on a Cu foil; (b) PMMA coated on the Gr/Cu; (c) Cu etched by immersing the PMMA/Gr/Cu sample in iron chloride solution for 1 h; (d) PMMA/Gr transferred on a PET substrate after a thorough cleaning; (e) growth of the ZnO-VANWs on the Gr/PET (after PMMA removal and Gr surface cleaning) in the seedless hydrothermal process with Gr facing down at 90 °C for 4 h in the zinc nitrate hexahydrate (10 mL) in ammonium hydroxide solution; (f) obtained ZnO-VANWs/Gr/PET nanohybrid; and (g) completed ZnO-VANWs/Gr/PET nanohybrid flexible sensors after encapsulation with PMMA.

factor of 389 in a so-called active-matrix sensor and 4800 in a piezoelectric potential gated MoS_2 field-effect transistor have been reported.[34] Sun *et al.* fabricated a ZnO NPs/Gr nanoplatelets (GNP) nanocomposite strain sensor exhibiting a G.F. ∼13 in the strain range of 0−44% and a dynamic response time of ∼0.5 s.[35] Chang *et al.* fabricated ZnO NWs/carbon black/PDMS nanocomposite strain sensors on a latex substrate and obtained a G.F. ∼25 with response time of ∼1.2 s.[23] Lee *et al.* fabricated a vertical nanohybrid strain sensor consisting of vertically aligned ZnO NWs (VANWs) grown on a ZnO-seeded layer (ZnO-SL) coated on the CNT-rGO bottom electrode on a polyethylene terephthalate (PET) substrate with a Au top electrode. A G.F. of 7.6 and response time of ∼0.2 s were obtained under different bending curvatures corresponding to a strain range of 0−6.2% on this Au/ZnO-VANWs/ZnO-SL/CNT-rGO sensor.[11]

In this work, we explore a new flexible strain sensor based on (0001)-oriented crystalline ZnO-VANW array fabricated on monolayer Gr grown using chemical vapor deposition (CVD) and transferred on PET substrates. A seedless hydrothermal process was developed for the growth of the ZnO-VANW array directly on the Gr/PET in a growth solution. The obtained ZnO-VANWs/Gr/PET strain sensor relies on the piezoelectric gating effect generated by deformed ZnO-VANWs on Gr, which leads to Gr channel conductivity modulation *via* gate-induced charge carrier doping to Gr. There are several advantages of this device. First, conductance change in only the Gr channel is measured, instead of that for the entire sample as in most nanocomposite strain sensors discussed above as an average effect. In addition, the combination of the monolayer CVD graphene with the (0001)-oriented crystalline ZnO-VANW array in this ZnO-VANWs/Gr/PET strain sensor allows an optimal piezoelectric gating effect (or strain sensitivity) to be obtained. Finally, this ZnO-VANWs/Gr/PET strain sensor can recognize the tensile and compressive strain on the ZnO-VANW array from the direction of the graphene's Dirac point shift. Indeed, a high G.F. up to ∼248 together with the opposite polarities of the Dirac point shift in response to upward/downward bending of the ZnO-VANWs/Gr/PET strain sensor were observed. In the following, we report our experimental results.

RESULT AND DISCUSSION

Figure 1 depicts schematically the entire process developed in this work for fabrication of the ZnO-VANWs/Gr/PET flexible strain sensors. Figure 1a,b shows the cross-sectional views of Gr on a Cu foil after the CVD growth and after coating PMMA on the Gr/Cu. Transfer of Gr consisted of etching out the Cu foil (Figure 1c) followed by attachment of Gr to a PET substrate with prefabricated Au/Ti electrodes (Figure 1d). Afterward, the sample was floated in the aqueous solution of mixed zinc nitrate hexahydrate and ammonium hydroxide (Figure 1e) with the Gr side facing down for growth of the ZnO-VANWs in the seedless hydrothermal process. A dense array of ZnO-VANWs (Figure 1f) can be obtained on a thoroughly cleaned CVD Gr surface with a careful control of the pH value ∼10 in the solution. In particular, the ZnO-VANWs obtained without a polycrystalline ZnO-SL deposited on Gr has a better interface with Gr by removing the charge traps in the defective ZnO-SL, which has been found to improve the photoresponsivity and response time in ZnO-VANWs/Gr ultraviolet detectors.[36,37] Therefore, this detrimental effect from a defective interface is expected to be minimized in the ZnO-VANWs/Gr/PET flexible strain sensors obtained using seedless hydrothermal growth. The final configuration of the ZnO-VANWs/Gr/PET nanohybrid flexible strain sensor is depicted schematically in Figure 1g after casting the PMMA passivation layer on the ZnO-VANWs/Gr/PET to provide mechanical stability to the device. It should be pointed out that the seedless hydrothermal growth method is facile, low-cost, and scalable for fabrication of the ZnO-VANWs/Gr/PET nanohybrid flexible strain sensors.

Figure 2a depicts an optical image of a ZnO-VANWs/Gr/PET flexible strain sensor mounted on a cylinder where one end of the sample is attached to the cylinder and another end is free to be bent for the bending test (Figure 2a). The four Au/Ti bars are used as electrodes for three strain sensors on the same sample for evaluation of the device performance consistency. The ZnO-VANWs/Gr channels for these three devices locate between the neighboring two Au/Ti bars. Figure 2b is a photograph of the side view of a ZnO-VANWs/Gr/PET flexible strain sensor held by a pair of tweezers, showing

https://dx.doi.org/10.1021/acsomega.0c03683
ACS Omega 2020, 5, 27359−27367

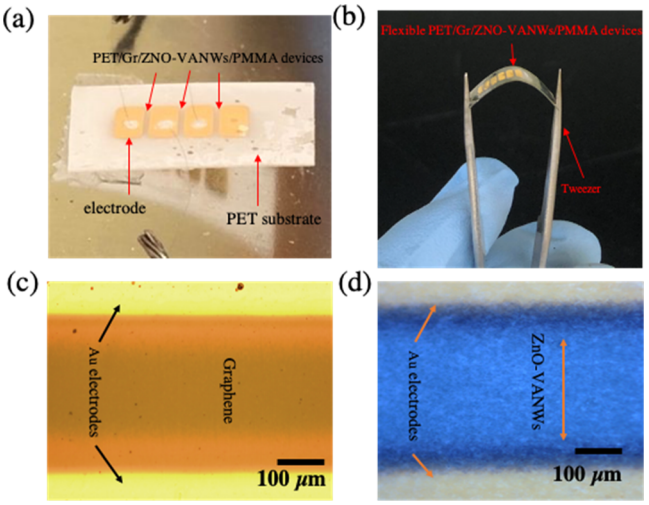

Figure 2. (a) Photograph of a sample of three ZnO-VANWs/Gr/PET flexible strain sensors mounted on the cylinder; (b) photograph of the side view of the same sample in (a), demonstrating the flexibility of the sample; optical images of the Gr channel (c) before and (d) after the ZnO-VANWs growth on the Gr channel.

the flexibility of the ZnO-VANWs/Gr/PET flexible strain sensors. The optical images of a representative transferred CVD Gr on the PET substrate before (Figure 2c) and after (Figure 2d) the ZnO-VANWs growth illustrate the uniformity of the sensor. Specifically, the uniform color contrast on both images suggests a uniform and clean Gr channel, as well a uniform distribution of translucent ZnO-VANWs on the Gr/PET.

Figure 3a shows the Raman spectra of Gr before (pristine, black) and after the hydrothermal ZnO-VANWs growth (red) on a Gr/PET. The characteristic Raman peaks of Gr, namely

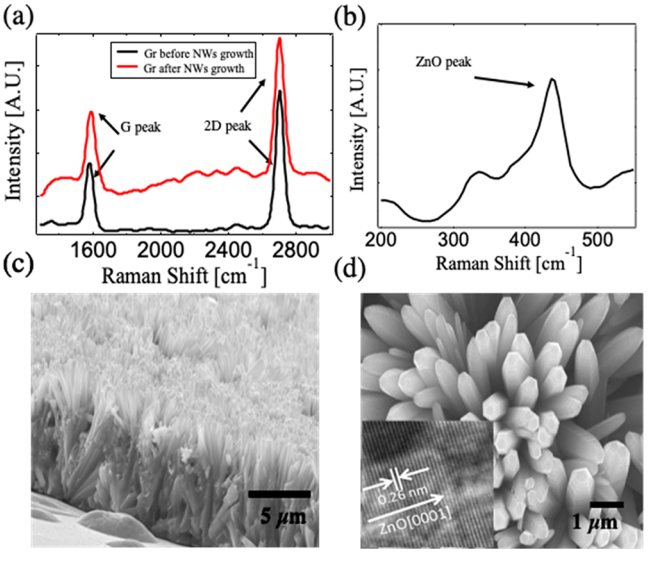

Figure 3. (a) Raman spectra of Gr before (black) and after the hydrothermal growth of ZnO-VANWs on Gr/PET (red); (b) Raman spectrum of ZnO-VANWs showing ZnO signature peak at 440 cm^{-1}; (c) SEM image of a ZnO-VANWs/Gr/PET sample at the 85° tilt angle with respect to the electron beam in SEM; and (d) top-view SEM image of a ZnO-VANWs/Gr/PET sample with the inset showing the HRTEM image of a representative crystalline ZnO-VANW.

the G peak at ~1590 cm^{-1} and 2D peak at ~2715 cm^{-1} can be observed on both spectra. The G peak corresponds to the E_g^2 phonon at the Brillouin zone center, and the 2D peak is related to the second-order harmonic of the D peak corresponding to the A_{1g} breathing mode of Gr.[38] On the pristine Gr (black) shown in Figure 3a, the Raman peak intensity ratio of 2D to G Raman peaks (I_{2D}/I_G) is around ~1.8, indicating that the CVD Gr used in this work is monolayer.[39,40] The D band at ~1354 cm^{-1} arising from defects in Gr is negligible. In fact, the ratio of the D to G peaks (I_D/I_G) is as low as ~1%. This indicates that the CVD Gr used in this work is high-quality monolayer CVD Gr. It is particularly worth pointing out that the quality of Gr was preserved in the seedless hydrothermal process for growth of the ZnO-VANWs, which is essential for the optimum performance of the ZnO-VANWs/Gr nanohybrid devices.[41] This is shown in Figure 3a (red spectrum) that the locations and symmetry of the Gr Raman signature peaks are preserved after the ZnO-VANW growth. A slightly reduced ratio of I_{2D}/I_G ~1.5 and the moderately increased D peak may be attributed to the presence of the ZnO-VANWs on top of Gr. In addition to the Raman signatures of Gr, the major Raman peak at ~440 cm^{-1} is attributed to the E_2 energy mode of ZnO, demonstrating the formation of crystalline ZnO-VANWs on Gr in the hydrothermal growth process as shown in Figure 3b.[42] Figure 3c shows the cross section of the ZnO-VANWs/Gr/PET taken at the tilt angle of 85° with respect to the electron beam in SEM, illustrating vertically aligned, dense ZnO nanowires on Gr/PET. The average length of ZnO-VANWs is 7.2 ± 1.4 μm. Figure 3d is the top view SEM image of the ZnO-VANW array, showing hexagonal-shaped cross section of the ZnO-VANWs with an average diameter of 460 ± 93 nm. The hexagonal shape suggests high crystallinity of the ZnO-VANWs, which was confirmed in the HRTEM study of the ZnO-VANWs. The inset of Figure 3d illustrates a HRTEM image of ZnO (0001) fringes perpendicular to the ZnO-NW axis with an average spacing of 0.26 nm, confirming the crystalline ZnO-VANW growth along the fast-growth direction of ZnO (0001) as soon as the ZnO nucleation occurs on Gr/PET. In order to form one-dimensional ZnO-VANWs, there are non-polar planes and polar planes, such as (0001) plane, in the wurtzite ZnO. Because of the fact that the surface energy along the (0001) plane is the lowest, (0001) ZnO nanowire growth is energetically preferred.[43]

Figure 4a illustrates the schematic of a compressive force applied on the ZnO-VANWs/Gr/PET strain sensor using a spring-loaded mechanical piston, and the inset (top) shows a photo of this apparatus having a spring constant of k = 1.23 N/mm obtained using the Hook's law given by $F = -k\Delta x$, where F and Δx are the force and change in spring length, respectively. Under the compression, the surface charges are developed at the two ends of the ZnO-VANWs as shown schematically in the inset (bottom) of Figure 4a. The compressive strain-induced surface charge at the ZnO-VANWs/Gr interface will induce a piezoelectric gating effect on the Gr channel and in turn change the channel conductivity. The strength of the piezoelectric gating effect induced is expected to be proportional to the applied force quantitatively.[44] Figure 4b compares the dynamic response $\Delta I = I - I_0$, defined as the change of the electric current in the Gr channel under a fixed bias voltage of 1.0 V with (I) and without (I_0) the applied force on the ZnO-VANWs/Gr/PET nanohybrid device. In Figure 4b, compression force pulses of 0.30 N (red) and 0.70 N (black) in amplitude were applied.

https://dx.doi.org/10.1021/acsomega.0c03683
ACS Omega 2020, 5, 27359−27367

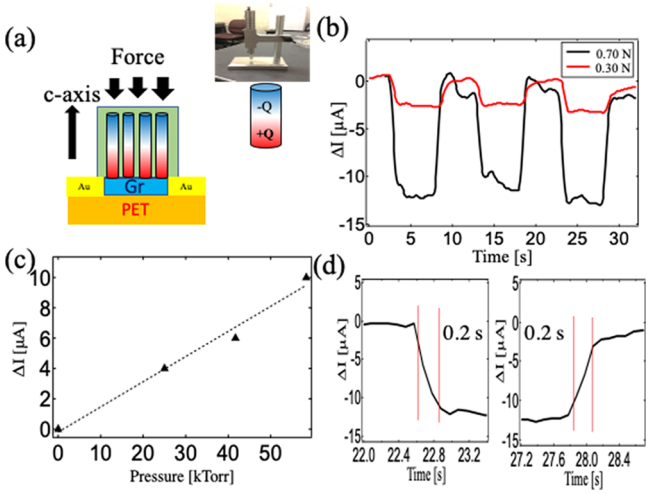

Figure 4. (a) Schematic of piezoelectric gating effect on the Gr channel induced by the compressive force on the ZnO-VANWs/Gr/PET strain sensors. Insets: photo of the spring-loaded apparatus (top) and distribution of the induced charges on a compressively deformed ZnO-VANW (bottom); (b) dynamic response ΔI of the ZnO-VANWs/Gr/PET strain sensor under pulsed compressive forces of 0.30 N (red) and 0.70 N (black). The bias voltage was 1.0 V. (c) ΔI *vs p* curve. (d) Mechanical response times extracted from (b) for the pulsed force of 0.70 N in amplitude.

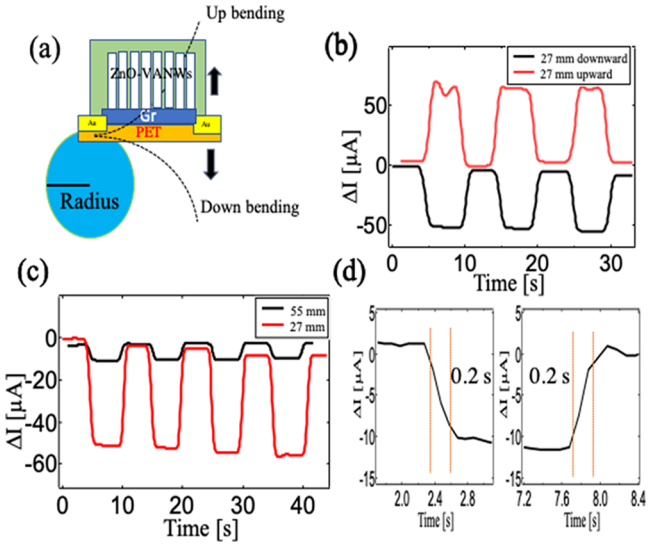

Figure 5. (a) Schematic of home-made bending setup; (b) dynamic response comparison of change in current for 27 mm for upward/downward bending; (c) dynamic response comparisons for bending radii of 55 and 27 mm; and (d) zoom-in images for depiction of rise/fall time.

Some low-level noises are visible in the ΔI measurement most probably caused by the disturbance of the Au/Ti electric contacts by the piston when the force pulses were applied. The amplitudes of ΔI are about 4 μA for 0.30 N and 10 μA for 0.70 N, respectively. Figure 4c depicts the amplitudes of ΔI as a function of the applied pressure amplitudes. The pressure is calculated by dividing the force by the area of the piston (9.0×10^{-7} m^2). The linear trend of the observed ΔI *versus p* curve illustrates the proportionality of the piezoelectric gating effect from the strain-induced ZnO/Gr interface charge (Q) which is proportional linearly to the applied force F ($Q = F \cdot g_{33}$), where g_{33} is the piezoelectric coefficient.[29] Figure 4d shows the zoom-in view of the ΔI in response to rise (left) and fall (right) of an applied force pulse of 0.70 N in amplitude. The strain rise (or fall) response time is defined as the period for the ΔI rising from 10 to 90% (or falling from 90 to 10%) of the response amplitude.[9] The strain response times obtained on the ZnO-VANWs/Gr/PET strain sensors are fairly symmetric with both rise and fall times of 0.20 s in the strain range studied in this work. Under different applied pulsed forces, the rise and fall times are approximately the same. The fast and symmetric response times can be attributed to a clean ZnO-VANWs/Gr interface with minimal charge traps. For all measurement, the bias voltage across the Gr channel was 1.0 V.

Figure 5a illustrates schematically the apparatus deployed for the bending test of the ZnO-VANWs/Gr/PET nanohybrid sensors mounted on a cylinder with one end of the sample attached to the cylinder and the other end set free for bending upward and downward. Figure 5b compares the dynamic response of the ZnO-VANWs/Gr/PET sensor to the downward (black) and upward (red) bending at a bending radius of 27 mm. Despite opposite polarities of the strain response, the ΔI amplitudes are comparable in the range of about 50−60 μA under the downward and upward bending directions. Figure 5c compares the dynamic responses taken at 55 mm (black) and 27 mm (red) bending radii with the ΔI amplitudes of 10 and 60 μA, respectively, indicating the smaller the bending radius, the larger the strain response. Figure 5d shows the zoomed-in views of a bend/release cycle with radius of curvature of 55 mm depicting the symmetric rise/fall times as 0.20 s/0.20 s. It should be pointed out that a shorter response time and higher strain sensitivity could be achieved if the crystallinity of the ZnO VANWs can be further improved to reduce charge trapping by defects in the ZnO nanowires. The defects in the ZnO NWs are affected directly by the nanowire growth conditions. For example, a response time of 10−20 ms was reported on the ZnO NW strain sensors reported grown using a vapor solid process at temperatures ∼1400 °C or higher.[45,46] This is not surprising since higher growth temperatures are favorable to obtain higher crystallinity and hence fewer defects. The ZnO growth temperature in hydrothermal processes is much lower, such as the work in this article (at 90 °C) and by others (95 °C).[47] In fact, similar response times of 0.2 s in the former and 0.13 s in the latter suggest that the lower crystallinity of ZnO nanowires may be a dominant reason for the longer response times. In addition, higher gauge factors up to 1250 were also achieved on Schottky devices using ZnO nanowires synthesized using high temperatures ∼1400 °C, suggesting a direct impact of ZnO crystallinity on the piezoelectric properties.[46] It should be realized that graphene may degrade at elevated temperatures of a few hundreds of Celsius in air or oxygen. Therefore, the low growth temperatures in hydrothermal process provide a unique resolution to accommodate ZnO nanowire growth directly on graphene. Nevertheless, further research is necessary to improve the crystallinity of the ZnO nanowires in hydrothermal processes for both higher strain sensitivity and response speed.

This polarity switch of strain response ΔI can be attributed to polarity change of the strain-induced charge at the ZnO-VANWs/Gr interface stemming from the switch between compressive and tensile strain applied on the ZnO-VANWs upon bending downward and upward of the ZnO-VANWs/Gr/PET nanohybrid sensors, respectively. This is illustrated

https://dx.doi.org/10.1021/acsomega.0c03683
ACS Omega 2020, 5, 27359−27367

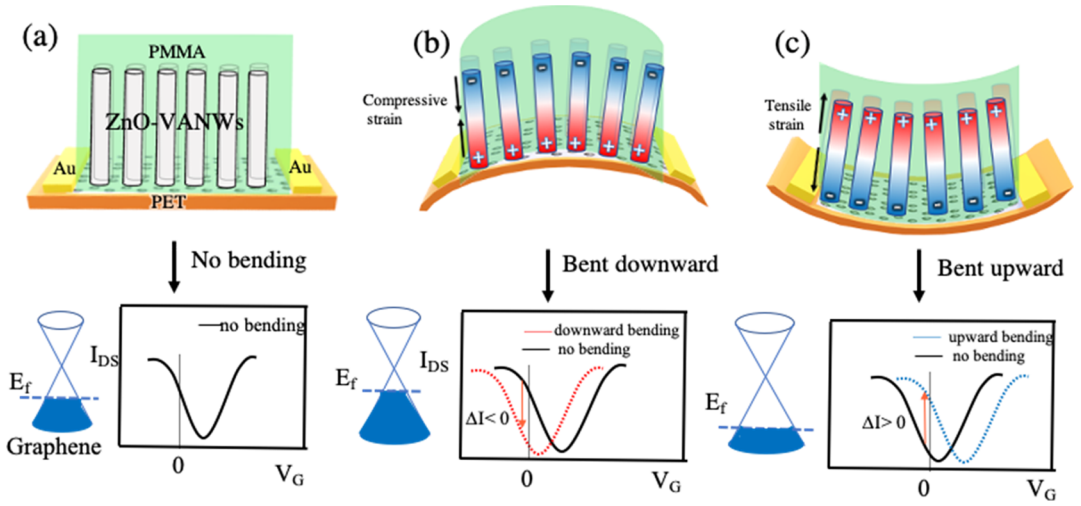

Figure 6. (a) Schematic of the ZnO-VANWs/Gr/PET strain sensor at zero strain (top) and the energy diagram of Gr along with the Gr channel drain-source current *vs* gate voltage $I_{DS}-V_G$ characteristic curve (bottom); (b) ZnO-VANWs/Gr/PET strain sensor under downward bending schematics with a compressive strain generated in the axial direction of the ZnO-NWs (top) and the left shift (n-doping) of the $I_{DS}-V_G$ curve and the Dirac point (bottom) with a negative ΔI illustrated by the red arrow; and (c) ZnO-VANWs/Gr/PET strain sensor under upward bending with a tensile strain generated in the axial direction of the ZnO-NWs (top) and the right shift (p-doping) of the $I_{DS}-V_G$ curve and Dirac point (bottom).

schematically in Figure 6. It should be pointed out that only a few ZnO nanowires are included in the schematic drawings of the ZnO-VANWs/Gr samples in Figure 6a–c under different bending conditions under no strain, downward bending and upward bending, respectively. For simplicity, each drawing only includes a few ZnO nanowires well separated to illustrate the details. Under no bending, the Dirac point (minimum I_{DS}) which is depicted by black dotted line located on the positive voltage side (above $V_G = 0$) since CVD Gr is typically p-doped in ambient,[48] which has been confirmed in our recent works on similar CVD Gr.[49−51] When the ZnO-VANWs/Gr/PET nanohybrid sensor is subjected to downward bending (Figure 6b), a compressive strain is applied to the ZnO-VANWs, resulting in positive charges generated at the ZnO-VANWs/Gr interface. This is equivalent to applying a fixed positive top-gate voltage in the double-gate graphene field-effect transistor.[50] A left shift of the Dirac point, or the minimum conductance point, will occur on the I_{sd} *versus* V_G curve when sweeping the back-gate voltage V_G (red curve) with respect to that for strain-free case (black curve). This means the Fermi energy of graphene (vertical dashed line at $V_G = 0$) will be shifted upward toward more n-doped[50,52] as shown in Figure 6b. This results in a negative strain response (or $\Delta I < 0$) as shown by the red arrow in Figure 6b. It should be pointed out that the negative strain response was also observed when a compressive force was applied to the ZnO-VANWs/Gr/PET nanohybrid sensor as shown in Figure 4b. In contrast, when the ZnO-VANWs/Gr/PET nanohybrid sensor is subjected to upward bending (Figure 6c), a tensile strain is applied along the ZnO-VANWs/Gr/PET nanohybrid sensor. The switch of the strain along the axial direction of the ZnO-VANWs from compressive to tensile leads to the ZnO-VANWs/Gr interface charge switch from positive to negative. This results in a right shift of the Dirac point (p-doping of Gr)[50,52] and hence a positive strain response (or $\Delta I > 0$) as shown in Figure 6c.

Figure 7a depicts the relative conductivity change of the Gr channel $\Delta\sigma/\sigma_0$ *versus* strain (ϵ) under downward bending. The strain was calculated using the formula $\epsilon = h/2R$, where h is the thickness of the substrate (200 μm for PET) and R is the

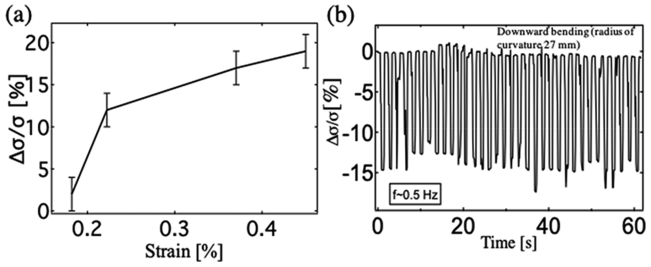

Figure 7. (a) Relative conductivity change of the Gr channel $\Delta\sigma/\sigma_0$ as function of the strain generated by downward bending of the ZnO-VANWs/Gr/PET flexible strain sensor and (b) multi-cycles of dynamic strain response to downward bending at the radius of curvature of 27 mm.

radius of curvature. The bending curvatures are 0.18, 0.23, 0.37, and 0.45 cm^{-1} respectively, at the radii of curvature of 55, 43, 27, and 22 mm for the bending experiment in this work. Based on the equation for the gauge factor G.F = $(\Delta\sigma/\sigma_0)/\epsilon$,[11] an average G.F. of ~67 is estimated from the slope of the linear curve fitting of the four data points in Figure 7a. At the lower limit of the strain, the G.F. is up to 248, which suggests a higher sensitivity at lower strains. This result suggests that the ZnO-VANWs/Gr/PET strain sensors are promising to detect low strains with high sensitivity. In Table 1, the performance of the ZnO-VANWs/Gr/PET nanohybrid sensors developed in this work is compared with that for several other flexible strain sensors based on the ZnO-NWs.[11,35,53,54] Overall, the ZnO-VANWs/Gr/PET nanohybrid sensors developed in this work show both improved G.F. and response speed (reduced response time). It is particularly worth mentioning that the average G.F. value of 67 in the ZnO-VANWs/Gr/PET sensor is 8.8 times higher than that of its counterpart of the Au/ZnO-VANWs/ZnO-SL/CNT-rGO sensor with a ZnO-SL for growth of the ZnO-VANWs.[11] In addition, the response time of 0.2 s in the former is an order of magnitude better than that of the latter. This improvement confirms the importance of the clean ZnO-VANWs/Gr interface for an effective transduction of the mechanical deformation on ZnO-VANWs to piezo-

https://dx.doi.org/10.1021/acsomega.0c03683
ACS Omega 2020, 5, 27359−27367

Table 1. Performance Comparison of ZnO Nanostructure/Gr Pressure/strain Sensor[a]

type	device	sensitivity $(\Delta\sigma/\sigma_0)/\epsilon$ (G.F.)	strain range (%)	RT (s)	references
PE	Gr/ZnO-VANWs	67−248	0−0.45	0.2	this work
PR	Au/ZnO-VANWs/ZnO-SL/CNT-rGO	7.6	0−6.2	2	11
resistive	CVD Gr/Au	42	0−20	1	54
PR	ZnO NP/GNP	13	0−44	0.5	35
PR	ZnO NWs/carbonblack	25	0−30	1.2	23

[a]PR-piezoresistive; PE-piezoelectric; RT-response time; GNP-graphene nanoplatelets.

electric gating on the Gr channel. Furthermore, the ZnO-VANWs/Gr/PET sensor can detect strain as low as 0.18% as shown in Figure 7a with very high G.F. = 248. The much-improved performance in the ZnO-VANWs/Gr/PET sensors is also associated with the underlying physics mechanism of piezoelectric gating for the strain sensing by measuring the Gr channel conductance change using a simple design of two electrodes, both on Gr. This is in contrast to vertical device structure in the Au/ZnO-VANWs/ZnO-SL/CNT-rGO sensor that requires fine control of the Au top electrode and CNT-rGO bottom electrode on the two ends of the ZnO-VANWs for measurement of the piezoelectric potential difference across the ZnO-NWs.[11] Figure 7b illustrates the multiple cycles of downward bending of the ZnO-VANWs/Gr/PET sensor with the radius of curvature of 27 mm. Despite a few spikes possibly caused by disturbance of the electrical contacts during the bending test, the strain response was reproducible, and no sign of sample damage could be seen. A better device design to protect the electric wiring of the sensor from the mechanical deformation is certainly necessary.

It should be noted that the strain detection in the ZnO-VANWs/Gr/PET devices is achieved through a combination of the piezoelectric field generated on the ZnO nanowires under mechanical deformation and a unique piezoelectric gating of graphene for the variation of graphene's conductivity. This strain sensing mechanism in the ZnO-VANWs/Gr/PET devices differs from that in most other strain sensors based on ZnO nanowires or other piezoelectric nanostructures reported in the literature. Specifically, the strain signal is measured on a single atomic sheet of graphene in the former in contrast to on the bulk of the sensor in the latter. Therefore, the ZnO-VANWs/Gr architecture could potentially enable very high strain sensitivity when optimized. In addition, the sensor electrodes of the ZnO-VANWs/Gr device are both on graphene, leading to a simpler device design as opposed to the ZnO nanowire Schottky strain sensors that require two different metal electrodes with one forming the Schottky junction and the other Ohmic contact with ZnO. Finally, ZnO-VANWs/Gr can be grown in solution at low temperatures typically below 100 °C in the hydrothermal process, leading to low-cost, scalable fabrication of the ZnO-VANWs/Gr devices on rigid as well as flexible substrates. However, the higher strain sensitivity, such as gauge factors exceeding 1200 on Schottky ZnO nanowires grown using vapor deposition methods at temperature exceeding 1400 °C, indicates that higher crystallinity of ZnO nanowires is important to the performance of ZnO-based strain sensors.[45,46] Therefore, further improvement of the crystallinity of the ZnO nanowires obtained in low-temperature hydrothermal process will be important to achieve higher performance of strain detection on ZnO-VANWs/Gr/PET samples.

CONCLUSIONS

In summary, we have developed a new ZnO-VANWs/Gr/PET nanohybrid flexible strain sensor using a facile fabrication process. This process consists of three major steps including: (1) CVD growth of monolayer graphene; (2) transfer of the CVD graphene on 200 μm thick flexible PET substrates with prefabricated Au/Ti electrodes; and (3) seedless hydrothermal growth of (0001)-oriented crystalline ZnO-VANW array directly on Gr to obtain ZnO-VANWs/Gr/PET with a clean ZnO-VANWs/Gr interface that is critical to achieving high piezoelectric gating on Gr channel for high strain sensitivity and high strain response speed. Under mechanical deformation either by applying the compressive pulsed forces normal to the sensor, or by bending the sensor up/down, the piezoelectric charge generated on the ZnO-VANWs/Gr interface provides the piezoelectric gating on the conductance of the Gr channel. High strain sensitivity and response speed have been obtained with an average G.F. up to 67 and response time (on/off) of 0.20 s/0.20 s in the strain range of 0.18−0.45%. At the lower strain limit of 0.18%, the sensor has a remarkably high G.F. = 248. Furthermore, this sensor has a clear recognition of the compressive and tensile strain on the ZnO-VANWs through a polarity switch of the ΔI from negative to positive due to the n-doping or p-doping of the Gr channel that shifts the Dirac point to left or right. The demonstrated high performance can be attributed to the combination of the most favorable (0001) oriented crystalline ZnO-VANWs and their clean interface with graphene formed in the seedless ZnO-VANW growth on graphene for realizing an optimal piezoelectric grating on graphene. Finally, the process developed for fabrication of the ZnO-VANWs/Gr/PET flexible sensors can be readily scaled up for low-cost commercial applications.

EXPERIMENTAL DETAILS

CVD of Monolayer Gr and Gr Transfer on PET Substrates. Monolayer Gr was grown at the temperature of 1050 °C and pressure of ∼1 Torr in a CVD furnace for 30 min on commercialized polycrystalline copper foils (25 μm in thickness, Sigma-Aldrich, USA). During the Gr growth, the flow of mixed gases of H_2 (7 SCCM) and CH_4 (40 SCCM) was maintained. The details of the CVD Gr growth were reported previously.[55,56] After the Gr growth, the furnace was shut down to allow the sample to cool down naturally to room temperature under the protection of 7 SCCM of H_2 flow. For Gr transfer, a Gr sample of 5 × 10 mm^2 was cut first and 3% PMMA was then spun-coated (3000 RPM for 1 min) onto one side of the Gr/Cu sample. The PMMA/Gr/Cu sample was baked afterward on a hot plate at 80 °C for 10 min. The PMMA/Gr/Cu sample was then soaked in iron chloride ($FeCl_3$) for 1 h to etch the Cu foil, and the resulted PMMA/Gr sample was thoroughly cleaned in deionized water (DI) following a protocol developed in our previous works.[51,57] A

https://dx.doi.org/10.1021/acsomega.0c03683
ACS Omega 2020, 5, 27359−27367

piece of PET substrate (thickness ~200 μm) of 6 × 14 mm^2 was cleaned using acetone, isopropyl alcohol (IPA), and DI water rinses. Afterward, Au (40 nm)/Ti (10 nm) electrodes were deposited through a shadow mask using electron-beam evaporation. Gr was then transferred onto PET with prefabricated Au/Ti electrodes, and PMMA was removed afterward by immersing the sample in acetone for approximately 1 h followed by 20 min in IPA. The Gr channel dimensions defined between the electrodes were 0.3 mm (length) × 3 mm (width). Typically, an array of 3 strain sensors were obtained on each sample with 4 Au/Ti electrodes for confirmation of the sensor performance.

ZnO-VANW Growth on Gr/PET in the Seedless Hydrothermal Process. The Gr/PET sample was floated in 100 mL of aqueous solution with Gr facing down. The growth of the ZnO-VANWs on Gr was carried out in an oven set at 90 °C for 4 h in the growth solution.[37,58] The aqueous solution was composed of 10 mL of zinc nitrate hexahydrate with ammonium hydroxide added under constant stirring to maintain the pH value to ~10.0 during the ZnO-VANW growth. A dense array of the ZnO-VANWs was obtained with the ZnO nanowire length typically in the range of 6−9 μm. It should be noted that a clean Gr surface and the constant pH value of ~10 are the key to dense and uniform nucleation and controlled growth of the ZnO-VANWs directly on Gr. After the ZnO-VANW growth, the ZnO-VANWs/Gr/PET sample was cleaned with DI water followed by nitrogen gas drying. A small drop of PMMA (3% in chloroform) was casted on the ZnO-VANWs/Gr/PET for mechanical stability.

Characterization of the ZnO-VANWs/Gr/PET Sample. The ZnO-VANWs/Gr/PET sample morphology was characterized using an optical microscope (Nikon Eclipse LV 150) and a scanning electron microscope (SEM, JEOL JSM-6380). The sample crystallinity was characterized using high-resolution transmission electron microscopy (HRTEM, FEI TF20XT) and Raman spectroscopy (WiTec alpha300) with the laser excitation wavelength of 488 nm. Electrical contact to the Au/Ti electrodes was completed using Pt wires 50 μm in diameter for device characterization. The current−voltage (I−V) characteristic and dynamic strain response of the ZnO-VANWs/Gr/PET nanohybrid flexible strain sensor under different applied strain by bending samples up/down to different radii of curvature were measured using a CHI660D electrochemical workstation. The compressive forces were applied using a spring-loaded mechanical piston having a spring constant of 1.23 N/mm, and the bending tests were performed by attaching the sample on cylinders with different radii of 22, 27, 43, and 55 mm, which correspond to bending curvatures of 0.45, 0.37, 0.23, and 0.18 cm^{-1}, respectively.

AUTHOR INFORMATION

Corresponding Authors

Mohan Panth − *Department of Physics and Astronomy, University of Kansas, Lawrence, Kansas 66045, United States;* orcid.org/0000-0002-4895-3527; Email: panthm@ku.edu

Judy Z. Wu − *Department of Physics and Astronomy, University of Kansas, Lawrence, Kansas 66045, United States;* Email: jwu@ku.edu

Authors

Brent Cook − *Department of Physics and Astronomy, University of Kansas, Lawrence, Kansas 66045, United States;* orcid.org/0000-0001-9288-7267

Mohammed Alamri − *Department of Physics and Astronomy, University of Kansas, Lawrence, Kansas 66045, United States;* orcid.org/0000-0002-7473-8644

Dan Ewing − *Department of Energy's Kansas City National Security Campus, Kansas City, Missouri 64147, United States*

Amy Wilson − *Department of Energy's Kansas City National Security Campus, Kansas City, Missouri 64147, United States*

Complete contact information is available at: https://pubs.acs.org/10.1021/acsomega.0c03683

Funding

This project is supported by Plant Directed Research and Development funds from the Department of Energy's National Security Campus operated and managed by Honeywell Federal Manufacturing and Technologies, LLC under contract no. DE-NA0002839. This research is also funded by NSF contracts nos. NSF-DMR-19094292 and NSF-ECCS-1809293/1809284 and ARO contract no. W911NF-16-1-0029.

Notes

The authors declare no competing financial interest.

ACKNOWLEDGMENTS

The authors thank the support by Plant Directed Research and Development funds from the Department of Energy's National Security Campus operated and managed by Honeywell Federal Manufacturing and Technologies, LLC under contract no. DE-NA0002839. This research was also funded by NSF contract nos. NSF-DMR-19094292 and NSF-ECCS-1809293/1809284 and ARO contract no. W911NF-16-1-0029.

REFERENCES

(1) Fan, F. R.; Tang, W.; Wang, Z. L. Flexible Nanogenerators for Energy Harvesting and Self-Powered Electronics. *Adv. Mater.* **2016**, *28*, 4283−4305.

(2) Misra, V.; Bozkurt, A.; Calhoun, B.; Jackson, T.; Jur, J.; Lach, J.; Lee, B.; Muth, J.; Oralkan, O.; Öztürk, M.; Trolier-McKinstry, S.; Vashaee, D.; Wentzloff, D.; Zhu, Y. Flexible technologies for self-powered wearable health and environmental sensing. *Proc. IEEE* **2015**, *103*, 665−681.

(3) Lee, M.; Chen, C.-Y.; Wang, S.; Cha, S. N.; Park, Y. J.; Kim, J. M.; Chou, L.-J.; Wang, Z. L. A hybrid piezoelectric structure for wearable nanogenerators. *Adv. Mater.* **2012**, *24*, 1759−1764.

(4) Giurgiutiu, V. *Structural Health Monitoring: With Piezoelectric Wafer Active Sensors*; Elsevier, 2007.

(5) Bhalla, S.; Yang, Y. W.; Zhao, J.; Soh, C. K. Structural health monitoring of underground facilities - Technological issues and challenges. *Tunn. Undergr. Space Technol.* **2005**, *20*, 487−500.

(6) Saudabayev, A.; Varol, H. A. Sensors for robotic hands: A survey of state of the art. *IEEE Access* **2015**, *3*, 1765−1782.

(7) Chen, Q.; Sun, Y.; Wang, Y.; Cheng, H.; Wang, Q.-M. ZnO nanowires-polyimide nanocomposite piezoresistive strain sensor. *Sens. Actuators, A* **2013**, *190*, 161−167.

(8) Alamusi; Hu, N.; Fukunaga, H.; Atobe, S.; Liu, Y.; Li, J. Piezoresistive strain sensors made from carbon nanotubes based polymer nanocomposites. *Sensors* **2011**, *11*, 10691−10723.

(9) Wang, X.; Liu, Z.; Zhang, T. Flexible sensing electronics for wearable/attachable health monitoring. *Small* **2017**, *13*, 1602790.

(10) Kanoun, O.; Müller, C.; Benchirouf, A.; Sanli, A.; Dinh, T.; Al-Hamry, A.; Bu, L.; Gerlach, C.; Bouhamed, A. Flexible carbon nanotube films for high performance strain sensors. *Sensors* **2014**, *14*, 10042−10071.

(11) Lee, T.; Lee, W.; Kim, S.-W.; Kim, J. J.; Kim, B.-S. Flexible textile strain wireless sensor functionalized with hybrid carbon nanomaterials supported ZnO nanowires with controlled aspect ratio. *Adv. Funct. Mater.* **2016**, *26*, 6206−6214.

(12) Wang, A. C.; Wu, C.; Pisignano, D.; Wang, Z. L.; Persano, L. Polymer nanogenerators: Opportunities and challenges for large-scale applications. *J. Appl. Polym. Sci.* **2018**, *135*, 45674.
(13) Karan, S. K.; Bera, R.; Paria, S.; Das, A. K.; Maiti, S.; Maitra, A.; Khatua, B. B. An Approach to Design Highly Durable Piezoelectric Nanogenerator Based on Self-Poled PVDF/AlO-rGO Flexible Nanocomposite with High Power Density and Energy Conversion Efficiency. *Adv. Energy Mater.* **2016**, *6*, 1601016.
(14) Chen, Y.-S.; Hsieh, G.-W.; Chen, S.-P.; Tseng, P.-Y.; Wang, C.-W. Zinc Oxide Nanowire-Poly(Methyl Methacrylate) Dielectric Layers for Polymer Capacitive Pressure Sensors. *ACS Appl. Mater. Interfaces* **2014**, *7*, 45−50.
(15) Bhavanasi, V.; Kumar, V.; Parida, K.; Wang, J.; Lee, P. S. Enhanced piezoelectric energy harvesting performance of flexible PVDF-TrFE bilayer films with graphene oxide. *ACS Appl. Mater. Interfaces* **2016**, *8*, 521−529.
(16) Tang, Y.; Zhao, Z.; Hu, H.; Liu, Y.; Wang, X.; Zhou, S.; Qiu, J. Highly Stretchable and Ultrasensitive Strain Sensor Based on Reduced Graphene Oxide Microtubes-Elastomer Composite. *ACS Appl. Mater. Interfaces* **2015**, *7*, 27432−27439.
(17) Chen, Z.; Wang, Z.; Li, X.; Lin, Y.; Luo, N.; Long, M.; Zhao, N.; Xu, J.-B. Flexible piezoelectric-induced pressure sensors for static measurements based on nanowires/graphene heterostructures. *ACS Nano* **2017**, *11*, 4507−4513.
(18) Kwon, J.; Seung, W.; Sharma, B. K.; Kim, S.-W.; Ahn, J.-H. A high performance PZT ribbon-based nanogenerator using graphene transparent electrodes. *Energy Environ. Sci.* **2012**, *5*, 8970−8975.
(19) Qiu, Y.; Zhang, H.; Hu, L.; Yang, D.; Wang, L.; Wang, B.; Ji, J.; Liu, G.; Liu, X.; Lin, J.; Li, F.; Han, S. Flexible piezoelectric nanogenerators based on ZnO nanorods grown on common paper substrates. *Nanoscale* **2012**, *4*, 6568−6573.
(20) Novoselov, K. S.; Geim, A. K.; Morozov, S. V.; Jiang, D.; Zhang, Y.; Dubonos, S. V.; Grigorieva, I. V.; Firsov, A. A. Electric field effect in atomically thin carbon films. *science* **2004**, *306*, 666−669.
(21) Zhao, J.; He, C.; Yang, R.; Shi, Z.; Cheng, M.; Yang, W.; Xie, G.; Wang, D.; Shi, D.; Zhang, G. Ultra-sensitive strain sensors based on piezoresistive nanographene films. *Appl. Phys. Lett.* **2012**, *101*, 063112.
(22) Ponnamma, D.; Guo, Q.; Krupa, I.; Al-Maadeed, M. A. S. A.; Varughese, K. T.; Thomas, S.; Sadasivuni, K. K. Graphene and graphitic derivative filled polymer composites as potential sensors. *Phys. Chem. Chem. Phys.* **2015**, *17*, 3954−3981.
(23) Chang, X.; Sun, S.; Sun, S.; Liu, T.; Xiong, X.; Lei, Y.; Dong, L.; Yin, Y. ZnO nanorods/carbon black-based flexible strain sensor for detecting human motions. *J. Alloys Compd.* **2018**, *738*, 111−117.
(24) Wang, Y.; Wang, A. X.; Wang, Y.; Chyu, M. K.; Wang, Q.-M. Fabrication and characterization of carbon nanotube-polyimide composite based high temperature flexible thin film piezoresistive strain sensor. *Sens. Actuators, A* **2013**, *199*, 265−271.
(25) Romano, G.; Mantini, G.; Carlo, A. D.; D'Amico, A.; Falconi, C.; Wang, Z. L. Piezoelectric potential in vertically aligned nanowires for high output nanogenerators. *Nanotechnology* **2011**, *22*, 465401.
(26) Han, W.; Zhou, Y.; Zhang, Y.; Chen, C.-Y.; Lin, L.; Wang, X.; Wang, S.; Wang, Z. L. Strain-Gated Piezotronic Transistors Based on Vertical Zinc Oxide Nanowires. *ACS Nano* **2012**, *6*, 3760−3766.
(27) Hinchet, R.; Lee, S.; Ardila, G.; Montès, L.; Mouis, M.; Wang, Z. L. Performance Optimization of Vertical Nanowire-based Piezoelectric Nanogenerators. *Adv. Funct. Mater.* **2014**, *24*, 971−977.
(28) Janotti, A.; Van de Walle, C. G. Fundamentals of zinc oxide as a semiconductor. *Rep. Prog. Phys.* **2009**, *72*, 126501.
(29) Wang, Z. L.; Song, J. Piezoelectric nanogenerators based on zinc oxide nanowire arrays. *Science* **2006**, *312*, 242−246.
(30) Chen, Y.; Gao, G.; Zhao, J.; Zhang, H.; Yu, J.; Yang, X.; Zhang, Q.; Zhang, W.; Xu, S.; Sun, J.; Meng, Y.; Sun, Q. Piezotronic graphene artificial sensory synapse. *Adv. Funct. Mater.* **2019**, *29*, 1900959.
(31) Yang, X.; Hu, G.; Gao, G.; Chen, X.; Sun, J.; Wan, B.; Zhang, Q.; Qin, S.; Zhang, W.; Pan, C.; Sun, Q.; Wang, Z. L. Coupled Ion-Gel Channel-Width Gating and Piezotronic Interface Gating in ZnO Nanowire Devices. *Adv. Funct. Mater.* **2019**, *29*, 1807837.
(32) Sun, Q.; Ho, D. H.; Choi, Y.; Pan, C.; Kim, D. H.; Wang, Z. L.; Cho, J. H. Piezopotential-Programmed Multilevel Nonvolatile Memory As Triggered by Mechanical Stimuli. *ACS Nano* **2016**, *10*, 11037−11043.
(33) Sun, Q.; Seung, W.; Kim, B. J.; Seo, S.; Kim, S.-W.; Cho, J. H. Active Matrix Electronic Skin Strain Sensor Based on Piezopotential-Powered Graphene Transistors. *Adv. Mater.* **2015**, *27*, 3411−3417.
(34) Zhao, J.; Wei, Z.; Zhang, Q.; Yu, H.; Wang, S.; Yang, X.; Gao, G.; Qin, S.; Zhang, G.; Sun, Q.; Wang, Z. L. Static and dynamic piezopotential modulation in piezo-electret gated MoS2 field-effect transistor. *ACS Nano* **2019**, *13*, 582−590.
(35) Sun, S.; Guo, L.; Chang, X.; Liu, Y.; Niu, S.; Lei, Y.; Liu, T.; Hu, X. A wearable strain sensor based on the ZnO/graphene nanoplatelets nanocomposite with large linear working range. *J. Mater. Sci.* **2019**, *54*, 7048−7061.
(36) Ashfold, M. N. R.; Doherty, R. P.; Ndifor-Angwafor, N. G.; Riley, D. J.; Sun, Y. The kinetics of the hydrothermal growth of ZnO nanostructures. *Thin Solid Films* **2007**, *515*, 8679−8683.
(37) Cook, B.; Liu, Q.; Liu, J.; Gong, M.; Ewing, D.; Casper, M.; Stramel, A.; Wu, J. Facile zinc oxide nanowire growth on graphene via a hydrothermal floating method: towards Debye length radius nanowires for ultraviolet photodetection. *J. Mater. Chem. C* **2017**, *5*, 10087−10093.
(38) Ferrari, A. C.; Basko, D. M. Raman spectroscopy as a versatile tool for studying the properties of graphene. *Nat. Nanotechnol.* **2013**, *8*, 235−246.
(39) Yogeswaran, N.; Navaraj, W. T.; Gupta, S.; Liu, F.; Vinciguerra, V.; Lorenzelli, L.; Dahiya, R. Piezoelectric graphene field effect transistor pressure sensors for tactile sensing. *Appl. Phys. Lett.* **2018**, *113*, 014102.
(40) Pan, G.; Li, B.; Heath, M.; Horsell, D.; Wears, M. L.; Al Taan, L.; Awan, S. Transfer-free growth of graphene on SiO2 insulator substrate from sputtered carbon and nickel films. *Carbon* **2013**, *65*, 349−358.
(41) Ferrari, A. C. Raman spectroscopy of graphene and graphite: Disorder, electron-phonon coupling, doping and nonadiabatic effects. *Solid State Commun.* **2007**, *143*, 47−57.
(42) Zheng, M. J.; Zhang, L. D.; Li, G. H.; Shen, W. Z. Fabrication and optical properties of large-scale uniform zinc oxide nanowire arrays by one-step electrochemical deposition technique. *Chem. Phys. Lett.* **2002**, *363*, 123−128.
(43) Hwang, J. O.; Lee, D. H.; Kim, J. Y.; Han, T. H.; Kim, B. H.; Park, M.; No, K.; Kim, S. O. Vertical ZnO nanowires/graphene hybrids for transparent and flexible field emission. *J. Mater. Chem.* **2011**, *21*, 3432−3437.
(44) Zhang, Y.; Liu, Y.; Wang, Z. L. Fundamental theory of piezotronics. *Adv. Mater.* **2011**, *23*, 3004−3013.
(45) Fei, P.; Yeh, P.-H.; Zhou, J.; Xu, S.; Gao, Y.; Song, J.; Gu, Y.; Huang, Y.; Wang, Z. L. Piezoelectric potential gated field-effect transistor based on a free-standing ZnO wire. *Nano Lett.* **2009**, *9*, 3435−3439.
(46) Zhou, J.; Gu, Y.; Fei, P.; Mai, W.; Gao, Y.; Yang, R.; Bao, G.; Wang, Z. L. Flexible piezotronic strain sensor. *Nano Lett.* **2008**, *8*, 3035−3040.
(47) Liao, X.; Yan, X.; Lin, P.; Lu, S.; Tian, Y.; Zhang, Y. Enhanced performance of ZnO piezotronic pressure sensor through electron-tunneling modulation of MgO nanolayer. *ACS Appl. Mater. Interfaces* **2015**, *7*, 1602−1607.
(48) Goniszewski, S.; Adabi, M.; Shaforost, O.; Hanham, S. M.; Hao, L.; Klein, N. Correlation of p-doping in CVD Graphene with Substrate Surface Charges. *Sci. Rep.* **2016**, *6*, 22858.
(49) Zhang, Y.; Hu, G.; Gong, M.; Alamri, M.; Ma, C.; Liu, M.; Wu, J. Z. Lateral Graphene p-n Junctions Realized by Nanoscale Bipolar Doping Using Surface Electric Dipoles and Self-Organized Molecular Anions. *Adv. Mater. Interfaces* **2019**, *6*, 1801380.
(50) Ma, C.; Lu, R.; Hu, G.; Han, J.; Liu, M.; Li, J.; Wu, J. Detecting Electric Dipoles Interaction at the Interface of Ferroelectric and Electrolyte Using Graphene Field Effect Transistors. *ACS Appl. Mater. Interfaces* **2017**, *9*, 4244−4252.

https://dx.doi.org/10.1021/acsomega.0c03683
ACS Omega 2020, 5, 27359−27367

(51) Xu, G.; Lu, R.; Liu, J.; Chiu, H.-Y.; Hui, R.; Wu, J. Z. Photodetection based on ionic liquid gated plasmonic Ag nanoparticle/graphene nanohybrid field effect transistors. *Adv. Opt. Mater.* **2014**, *2*, 729−736.
(52) Hu, G.; Wu, J.; Ma, C.; Liang, Z.; Liu, W.; Liu, M.; Wu, J. Z.; Jia, C.-L. Controlling the Dirac point voltage of graphene by mechanically bending the ferroelectric gate of a graphene field effect transistor. *Mater. Horiz.* **2019**, *6*, 302−310.
(53) Gullapalli, H.; Vemuru, V. S. M.; Kumar, A.; Botello-Mendez, A.; Vajtai, R.; Terrones, M.; Nagarajaiah, S.; Ajayan, P. M. Flexible Piezoelectric ZnO-Paper Nanocomposite Strain Sensor. *Small* **2010**, *6*, 1641−1646.
(54) Chun, S.; Choi, Y.; Park, W. All-graphene strain sensor on soft substrate. *Carbon* **2017**, *116*, 753−759.
(55) Liu, J.; Xu, G.; Rochford, C.; Lu, R.; Wu, J.; Edwards, C. M.; Berrie, C. L.; Chen, Z.; Maroni, V. A. Doped graphene nanohole arrays for flexible transparent conductors. *Appl. Phys. Lett.* **2011**, *99*, 023111.
(56) Xu, G.; Liu, J.; Wang, Q.; Hui, R.; Chen, Z.; Maroni, V. A.; Wu, J. Plasmonic Graphene Transparent Conductors. *Adv. Mater.* **2012**, *24*, OP71−OP76.
(57) Lu, R.; Liu, J.; Luo, H.; Chikan, V.; Wu, J. Z. Graphene/GaSe-nanosheet hybrid: towards high gain and fast photoresponse. *Sci. Rep.* **2016**, *6*, 19161.
(58) Liu, J.; Lu, R.; Xu, G.; Wu, J.; Thapa, P.; Moore, D. Development of a Seedless Floating Growth Process in Solution for Synthesis of Crystalline ZnO Micro/Nanowire Arrays on Graphene: Towards High-Performance Nanohybrid Ultraviolet Photodetectors. *Adv. Funct. Mater.* **2013**, *23*, 4941−4948.

https://dx.doi.org/10.1021/acsomega.0c03683
ACS Omega 2020, 5, 27359−27367